Interpretable Local-to-Global Estimation of Brain Aging Speed From Morphological Changes Using Longitudinal Structural MRI Data

Yuanwang Zhang[1], Hongming Li[2], and Yong Fan[2,✉]

[1] Department of Bioengineering, School of Engineering and Applied Science, University of Pennsylvania, Philadelphia PA 19104, USA
ywzhang3@seas.upenn.edu
[2] Department of Radiology, Perelman School of Medicine, University of Pennsylvania, Philadelphia PA 19104, USA
{Hongming.Li,Yong.Fan}@pennmedicine.upenn.edu

Abstract. Accurate characterization of brain aging is essential for understanding cognitive decline and assessing the risk of neurodegenerative disease. Brain age estimated from cross-sectional magnetic resonance imaging (MRI) data provides a snapshot of brain health relative to chronological age, and the derived brain age delta has emerged as a promising biomarker. However, brain age delta reflects cumulative effects at a single time point and fails to capture ongoing aging dynamics. Longitudinal approaches address this limitation by estimating age differences between scan pairs to derive aging speed. Nevertheless, existing methods primarily rely on intensity or texture differences between images, overlook the spatial heterogeneity of aging processes, and provide limited interpretability. To overcome these limitations, we propose a novel framework that estimates brain aging speed from longitudinal deformation fields obtained via diffeomorphic image registration. Instead of solely generating a single global estimate, our method produces patch-wise local aging predictions and adaptively integrates them into a unified global prediction, improving both predictive performance and interpretability. Evaluated on large-scale datasets, our approach achieves superior accuracy compared with existing methods and enhances the identification of abnormal aging patterns in diseased populations. Code is available at https://github.com/Kateridge/MorphologyAgingSpeed.

Keywords: Brain aging modeling · Interpretability · Longitudinal MRI

1 Introduction

Brain aging is a complex and long-term process characterized by gradual cognitive decline and biological changes such as weakened neuronal communication and regional brain atrophy. While normal aging follows relatively consistent trajectories, neurodegenerative diseases often induce abnormal regional atrophy patterns [18,20]. Understanding normal aging trajectories is therefore critical for

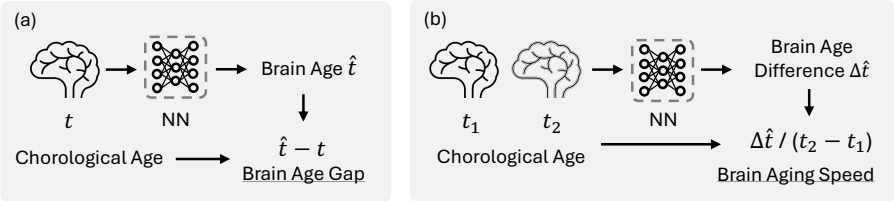

Fig. 1. (a) Conventional cross-sectional brain age modeling predicts brain age from a single MRI scan. Brain age delta is defined as the difference between the predicted brain age and the chronological age. (b) Longitudinal brain aging modeling predicts the age difference between two MRI scans. Brain aging speed is computed as the predicted brain age difference normalized by the chronological time interval between scans.

elucidating neurodegenerative disease progression and enabling precise diagnosis and personalized interventions.

Brain age has emerged as a promising imaging biomarker for quantifying biological aging, typically estimated from MRI scans [8,4,12]. As illustrated in Fig. 1(a), brain age models are commonly trained on healthy individuals, and the difference between predicted brain age and chronological age, often referred to as the brain age delta, is used as an indicator of brain health. A positive delta is generally interpreted as accelerated aging [2]. However, recent studies suggest that brain age delta does not necessarily reflect accelerated aging, as brain age models built upon cross-sectional data primarily capture group-level averages of the training data and are not equipped to account for individual variability in aging rate [19]. For instance, an individual may consistently exhibit a positive delta over time, reflecting a stable baseline shift rather than an increased ongoing aging rate.

Longitudinal studies provide a promising alternative for estimating aging dynamics by modeling temporal changes in brain imaging data. Recent approaches predict age differences directly from paired T1-weighted MRI scans [22,9], from which brain aging speed is computed as the ratio of the predicted age difference and the chronological time interval (Fig. 1(b)). However, existing methods primarily rely on intensity-based differences between MRI scans, making them sensitive to imaging artifacts and scanner variability. In addition, they typically yield a single global prediction, overlooking the spatial heterogeneity of brain aging patterns [12]. This can lead to suboptimal performance and reduce interpretability regarding region-specific contributions.

To overcome these limitations, we propose a novel framework that jointly characterizes local and global brain aging dynamics through morphology-driven modeling (Fig. 2). To derive representations more closely related to biological aging, we first estimate longitudinal morphological changes using diffeomorphic image registration, yielding a smooth, topology-preserving deformation field that describes anatomical transformations between scans [14]. We then compute the Jacobian determinant of the deformation field to quantify voxel-wise expansion and contraction. To account for the spatial heterogeneity of aging dynamics, in-

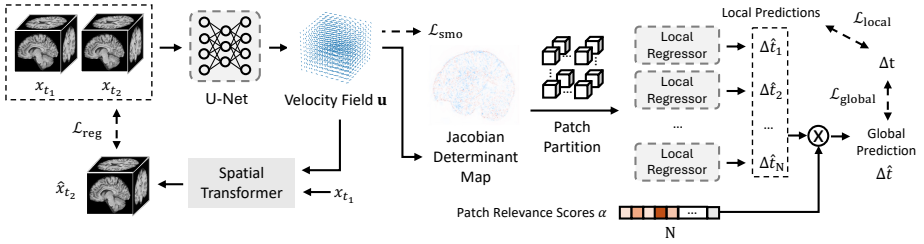

Fig. 2. Overview of Local-to-Global Estimation of Brain Aging Speed. Longitudinal morphological changes are first estimated using deep learning–based diffeomorphic image registration, producing a Jacobian determinant map that represents voxel-wise expansion or contraction. The Jacobian map is then partitioned into non-overlapping patches, and each patch is processed by a dedicated local regressor to predict regional aging speed. The local predictions are subsequently integrated using learned patch relevance scores, yielding a global prediction and an interpretable measure of each patch's contribution.

stead of producing a single global prediction, we partition the Jacobian map into non-overlapping patches and assign each patch to a dedicated local regressor to estimate regional brain age differences. These local predictions are subsequently integrated using learned patch relevance scores to generate a global age difference estimate [11]. This design captures spatially varying aging patterns while enhancing both predictive performance and local interpretability.

Our contribution are as follows: 1) We propose a morphology-driven framework that estimates brain aging speed from registration-derived deformation fields; 2) We introduce a patch-wise regression strategy that jointly produces local and global predictions, accounting for spatial heterogeneity while enhancing interpretability; 3) We validate our method on a large and diverse dataset, demonstrating improved prediction performance and effectiveness in identifying abnormal aging patterns in diseased populations.

2 Method

In this section, we present the proposed aging speed estimation framework, as shown in Fig. 2. Given a pair of MRI scans, x_{t_1} and x_{t_2}, acquired from two visits of the same subject at chronological ages $t_1 < t_2$, our goal is to learn a mapping that predicts the age difference $\Delta\hat{t}$ between the two scans. The model is trained on cognitively unimpaired subjects to capture normative aging dynamics. When applied to new data, the aging speed v is defined as the ratio between the predicted age difference and the actual chronological interval: $v = \Delta\hat{t}/\Delta t = \Delta\hat{t}/(t_2 - t_1)$. Intuitively, $v = 1$ corresponds to normal aging, whereas $v > 1$ indicates accelerated aging.

Modeling morphological changes. We model longitudinal morphological changes between x_{t_1} and x_{t_2} using diffeomorphic image registration that is implemented with a deep neural network [14]. Specifically, x_{t_1} and x_{t_2} are concatenated and fed into a U-Net to predict a stationary velocity field $u : \Omega \to \mathbb{R}^3$, where $\Omega \subset \mathbb{R}^3$ denotes the image domain. In discrete form, $u \in \mathbb{R}^{3\times \mathrm{H}\times \mathrm{W}\times \mathrm{D}}$ with a three-dimensional velocity vector defined at each voxel of the input images. The corresponding diffeomorphic deformation field $\phi : \Omega \to \Omega$ is obtained by integrating the ordinary differential equation parameterized by u:

$$\frac{d(\phi^{(t)})}{dt} = u(\phi^{(t)}), \phi^{(0)} = \mathrm{Id}. \tag{1}$$

Integrating Eq. 1 over unit time yields the final deformation field:

$$\phi = \int_0^1 u(\phi^{(t)})dt. \tag{2}$$

A spatial transformer layer [13] is then used to warp x_{t_1} using ϕ to align it with x_{t_2}. Registration accuracy is enforced using a local normalized cross-correlation loss [3] $\mathcal{L}_{reg}$ between the warped image $\hat{x}_{t_2} = x_{t_1} \circ \phi$ and x_{t_2}. Following [5], a smoothness regularization loss $\mathcal{L}_{smo}$ is further applied to the velocity field u using a diffusion regularizer on its spatial gradients.

The deformation field encodes the voxel-wise displacement from x_{t_1} to x_{t_2}, with a displacement vector defined at each voxel. To quantify the corresponding local volumetric changes, we compute the Jacobian determinant map $J \in \mathbb{R}^{\mathrm{H}\times \mathrm{W}\times \mathrm{D}}$ of the deformation field ϕ, which characterizes voxel-wise expansion ($J > 1$) or contraction ($J < 1$). This Jacobian map serves as a morphology-based representation of longitudinal brain changes for subsequent aging speed estimation.

Local predictions. Because aging is spatially heterogeneous and different brain regions may exhibit distinct aging patterns, we partition the Jacobian determinant map into N non-overlapping patches $J_i, i \in [1, \mathrm{N}]$. A patch-specific regression model is built for each patch to estimate the local brain age difference $\hat{\Delta t_i}$. To encourage local predictions to approximate the true chronological age difference $\Delta t = t_2 - t_1$, we use the mean absolute error (MAE) loss:

$$\mathcal{L}_{local} = \frac{1}{\mathrm{N}} \sum^{\mathrm{N}} |\hat{\Delta t_i} - \Delta t|. \tag{3}$$

Global prediction. The global prediction $\hat{\Delta t}$ is obtained by aggregating local predictions using a set of patch relevance scores α_i:

$$\hat{\Delta t} = \sum^{\mathrm{N}} \alpha_i \hat{\Delta t_i}. \tag{4}$$

Table 1. Summary of cognitive unimpaired participants used to train and validate the framework. The numbers of subjects, sessions, and image pairs are reported, together with the statistics of Δt, t_1, and t_2 (measured in years).

Cohort	N	N	N	Δt in pairs	Age (t_1)				Age (t_2)			
	(subjects)	(sessions)	(pairs)	mean(std)	min.	max.	mean (std)		min.	max.	mean (std)	
ADNI	562	2576	5544	3.9 (2.6)	55.8	94.6	75.4 (6.1)		57.2	95.6	79.4 (6.4)	
OASIS-3	439	1339	1630	4.7 (2.5)	43.4	92.3	66.2 (8.4)		46.7	94.4	70.9 (8.2)	
AIBL	155	502	657	2.7 (1.4)	61.0	90.3	73.2 (6.8)		62.6	92.4	76.0 (6.8)	

The relevance weights α_i are set as learnable parameters and are jointly optimized with other model parameters. To ensure non-negativity and unit summation, the Softmax function is applied to the relevance scores. The global prediction is also supervised with the MAE loss:

$$\mathcal{L}_{global} = |\Delta\hat{t} - \Delta t|. \tag{5}$$

The final objective is a weighted sum of the registration loss, smoothness loss, local prediction loss, and global prediction loss: $\mathcal{L} = 1.0 * \mathcal{L}_{reg} + 0.01 * \mathcal{L}_{smo} + 1.0 * \mathcal{L}_{local} + 1.0 * \mathcal{L}_{global}$.

3 Experiments

Datasets and participants. Longitudinal T1-weighted MRI scans were collected from three cohorts: the Alzheimer's Disease Neuroimaging Initiative (ADNI) [16], Open Access Series of Imaging Studies (OASIS-3) [10], and Australian Imaging Biomarkers and Lifestyle Study of Aging (AIBL) [6]. A total of 3915 imaging sessions from 1001 cognitively unimpaired (CU) subjects were used to train the proposed framework. Each subject had at least two sessions, and all sessions had valid age and diagnosis information. A subject was defined as CU if all of their sessions were consistently labeled as cognitively unimpaired. For each subject, all possible image pairs were constructed with chronological age differences ranging from 1 to 16 years. The ADNI and OASIS-3 cohorts were randomly split at the subject level into training (3087 sessions from 795 subjects, 5539 image pairs), validation (343 sessions from 94 subjects, 544 image pairs), and internal test sets (485 sessions from 112 subjects, 1091 image pairs). The AIBL cohort was used as an independent external test set (502 sessions from 155 subjects, 657 image pairs) to evaluate model generalizability. Subject-level splitting was performed to ensure that images from the same subject did not appear in multiple data partitions. A summary of the dataset is provided in Table 1.

MRI preprocessing. All MRIs were preprocessed using standardized steps, including bias field correction [21] and affine registration to align each image to MNI space [1] defined by the ICBM 2009c nonlinear symmetric template [7]. To reduce computational burden, the processed images were cropped to remove background, resulting in an image resolution of $176 \times 192 \times 176$.

Table 2. Performance comparison with existing methods and ablation models. Evaluation metrics include mean absolute error (MAE), root mean squared error (RMSE), and coefficient of determination (R^2). Best performance is highlighted in **bold**.

Methods	Longitudinal	Internal Test			External Test		
		MAE ↓	RMSE ↓	R^2 ↑	MAE ↓	RMSE ↓	R^2 ↑
SFCN [15]	✗	2.35	3.21	0.26	1.41	1.79	0.26
LM [22]	✓	1.47	2.03	0.58	0.96	1.30	0.32
LILAC [9]	✓	1.66	2.77	0.36	0.96	1.29	0.51
Ours (w/o morphological changes)	✓	1.25	1.81	0.60	0.83	1.11	0.50
Ours (w/o local predictions)	✓	1.33	1.77	0.58	0.87	1.23	0.56
Ours	✓	**1.13**	**1.59**	**0.68**	**0.70**	**0.94**	**0.60**

Implementation details. We adopted the U-Net architecture from [17]. The local regressors were implemented using a lightweight CNN backbone [15]. Model training was performed using the Adam optimizer with a learning rate of 10^{-3} and a batch size of 8. The framework was trained for 100 epochs, requiring approximately 40 hours on an NVIDIA A40 GPU. To balance predictive performance and computational efficiency, the Jacobian determinant map was partitioned into $4 \times 4 \times 4 = 64$ non-overlapping patches.

Comparison with existing methods and ablation experiments. We compared the proposed method with: (1) SFCN [15], a widely used cross-sectional brain age prediction model, with the age differences computed as the difference between two individual predictions; (2) LM [22], which estimates age differences from voxel-level differences between paired scans; and (3) LILAC [9], which predicts age differences using feature-level differences between paired scans. In addition, two ablated versions of our framework were evaluated: (4) a variant that replaces the Jacobian determinant map with raw image differences while retaining the local prediction module (w/o morphological changes); and (5) a variant that performs global prediction only using the Jacobian determinant map without the local prediction module (w/o local prediction).

As shown in Table 2, longitudinal methods (LM, LILAC, and ours) substantially outperformed the cross-sectional approach (SFCN). Incorporating morphological information to predict temporal changes (Ours w/o local predictions) consistently improved performance on both internal and external test sets. Similarly, accounting for spatial heterogeneity via local predictions (Ours w/o morphological changes) also led to consistent gains. Integrating both components in the full framework further enhanced performance.

Effects of patch size. We evaluated the impact of patch size on model performance using three partition settings: $2 \times 2 \times 2$ patches, $4 \times 4 \times 4$ patches, and $6 \times 6 \times 6$ patches, where the Jacobian determinant map is evenly divided along the three spatial dimensions. Smaller patch sizes generally provide finer-grained interpretability. However, experimental results (Table 3) show that excessively increasing the number of patches may degrade performance, likely due to the

Table 3. Effects of patch size on prediction performance. The Jacobian determinant map is evenly divided along the three spatial dimensions into a specified number of patches. Best performance is highlighted in **bold**.

Number of Patches	Internal Test			External Test		
	MAE ↓	RMSE ↓	R^2 ↑	MAE ↓	RMSE ↓	R^2 ↑
$2 \times 2 \times 2$	**1.10**	**1.46**	0.65	0.86	1.10	0.57
$4 \times 4 \times 4$	1.13	1.59	**0.68**	**0.70**	**0.94**	**0.60**
$6 \times 6 \times 6$	1.31	1.97	0.51	0.73	0.99	0.57

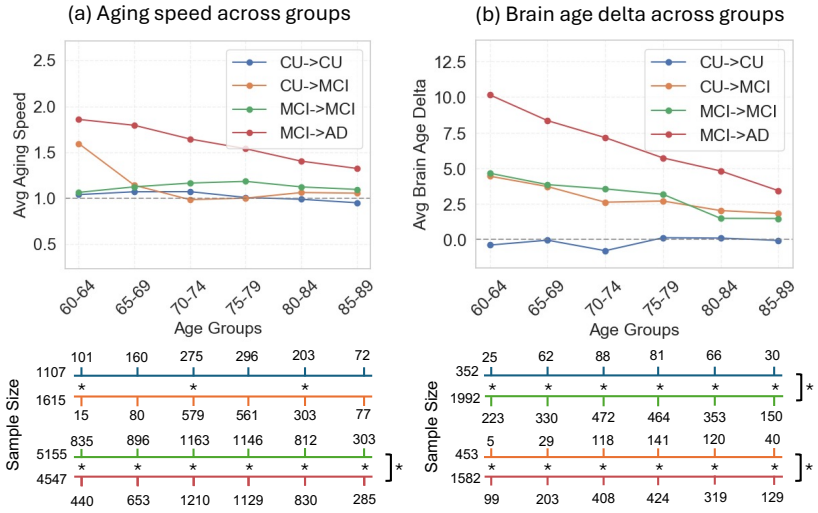

Fig. 3. Trends of brain aging speed and brain age delta across progression and non-progression groups. Subjects are stratified into age bins, and average values are computed within each bin. Colors denote different groups. Sample sizes for each group and age bin are shown, along with Wilcoxon rank-sum test results comparing progression and non-progression groups. Asterisks indicate $p < 0.05$.

increased model complexity as each patch is associated with an independent local regressor. To balance interpretability, predictive performance, and computational efficiency, we select $4 \times 4 \times 4$ patch partitions for subsequent experiments.

Aging speed in disease populations. To validate the proposed method for modeling aging dynamics and detecting abnormal aging patterns, we applied the trained model to diagnostic transition groups defined by changes in diagnosis between the first and last visits, including two non-progression groups (CU-to-CU, MCI-to-MCI), and two progression groups (CU-to-MCI, MCI-to-AD).

Aging speed was computed as $\Delta\hat{t}/(t_2 - t_1)$, and the age-related trend in average aging speed is shown in Fig. 3(a). For comparison, brain age delta was derived from SFCN predictions as a cross-sectional biomarker and is shown in

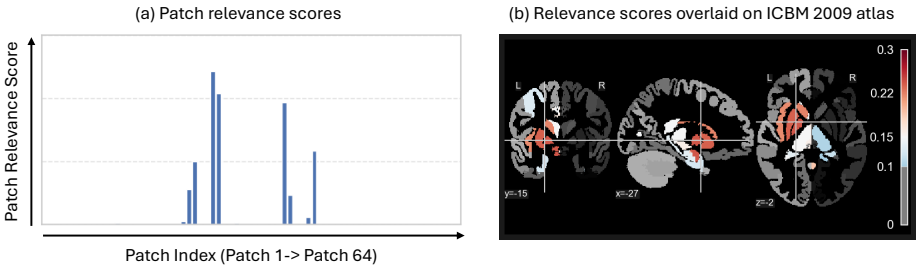

Fig. 4. Visualization of learned patch relevance scores. (a) Distribution of patch relevance scores, where the x-axis represents patch indices and the y-axis represents relevance score values. (b) Brain region visualization obtained by projecting patch relevance scores onto the ICBM 2009 atlas. When a brain region overlaps with multiple patches, the regional score is computed as the average score of the overlapping patches.

Fig. 3(b). The non-progression groups (CU-to-CU and MCI-to-MCI) exhibited relatively constant aging speeds close to 1.0, suggesting stable aging dynamics. In contrast, the progression groups (CU-to-MCI and MCI-to-AD) showed higher aging speeds, indicating accelerated aging. For brain age delta, the CU-to-CU group had values centered around 0, whereas other groups involving cognitively impaired or diseased subjects showed consistently positive values. We further observed significant Spearman correlations between brain aging speed and longitudinal cognitive changes in MMSE ($r = -0.23$), CDR ($r = 0.28$), FAQ ($r = 0.24$), and ADAS13 ($r = 0.23$), with all $p < 0.001$.

Together, these results suggest that the proposed aging speed measure and conventional brain age delta capture complementary aspects of brain aging. Brain age delta appears to reflect cumulative brain abnormality or disease-related deviation at a given visit, as shown by consistently positive values in impaired or progressing groups. In contrast, aging speed explicitly captures the rate of longitudinal changes and is therefore more directly related to ongoing disease progression.

Region contributions. We visualized the learned patch relevance scores and projected them onto the ICBM 2009 brain atlas to improve interpretability, as shown in Fig. 4. The model learned sparse relevance patterns without explicit sparsity regularization, suggesting that only a subset of regions contributed substantially to aging speed prediction. In particular, subcortical regions showed relatively high relevance scores, indicating that they may play an important role in modeling longitudinal aging dynamics.

4 Discussion and Conclusions

In this paper, we proposed a morphology-driven framework for estimating brain aging speed from longitudinal MRI scans. Unlike conventional brain age mod-

els that rely on cross-sectional and intensity-based representations, our method leverages diffeomorphic image registration to capture anatomical deformation patterns and uses Jacobian determinant maps to characterize voxel-wise morphological changes. By further incorporating a patch-wise regression strategy, the proposed framework jointly models local and global aging dynamics, improving predictive performance while providing interpretability regarding regional contributions. Experimental results on large-scale longitudinal datasets demonstrate that the proposed approach outperforms existing cross-sectional and longitudinal methods in accuracy and can identify abnormal aging patterns in populations with cognitive impairment.

Nevertheless, several limitations should be acknowledged. The proposed framework does not explicitly account for potential confounding factors such as age and sex, which may limit its ability to fully characterize the complex and nonlinear dynamics of brain aging. Future work will focus on developing more flexible modeling strategies that jointly account for these confounders to improve the accuracy, robustness, and generalizability of aging speed estimation.

Acknowledgments. This work was supported in part by the National Institutes of Health under grants R01AG066650 and R01AG054409.

Disclosure of Interests. The authors declare that they have no known competing financial interests or personal relationships that could have appeared to influence the work reported in this paper.

References

1. Avants, B.B., Tustison, N.J., Stauffer, M., Song, G., Wu, B., Gee, J.C.: The insight toolkit image registration framework. Frontiers in neuroinformatics **8**, 44 (2014)
2. Baecker, L., Garcia-Dias, R., Vieira, S., Scarpazza, C., Mechelli, A.: Machine learning for brain age prediction: Introduction to methods and clinical applications. EBioMedicine **72** (2021)
3. Balakrishnan, G., Zhao, A., Sabuncu, M.R., Guttag, J., Dalca, A.V.: Voxelmorph: a learning framework for deformable medical image registration. IEEE transactions on medical imaging **38**(8), 1788–1800 (2019)
4. Cole, J.H., Poudel, R.P., Tsagkrasoulis, D., Caan, M.W., Steves, C., Spector, T.D., Montana, G.: Predicting brain age with deep learning from raw imaging data results in a reliable and heritable biomarker. NeuroImage **163**, 115–124 (2017)
5. Dalca, A.V., Balakrishnan, G., Guttag, J., Sabuncu, M.R.: Unsupervised learning of probabilistic diffeomorphic registration for images and surfaces. Medical image analysis **57**, 226–236 (2019)
6. Ellis, K.A., Bush, A.I., Darby, D., De Fazio, D., Foster, J., Hudson, P., et al.: The Australian imaging, biomarkers and lifestyle (AIBL) study of aging: methodology and baseline characteristics of 1112 individuals recruited for a longitudinal study of Alzheimer's disease. International psychogeriatrics **21**(4), 672–687 (2009)
7. Fonov, V., Evans, A.C., Botteron, K., Almli, C.R., McKinstry, R.C., Collins, D.L., Group, B.D.C., et al.: Unbiased average age-appropriate atlases for pediatric studies. Neuroimage **54**(1), 313–327 (2011)

8. Franke, K., Ziegler, G., Klöppel, S., Gaser, C.: Estimating the age of healthy subjects from T1-weighted MRI scans using kernel methods: exploring the influence of various parameters. Neuroimage **50**(3), 883–892 (2010)
9. Kim, H., Karaman, B.K., Zhao, Q., Wang, A.Q., Sabuncu, M.R., Alzheimer's Disease Neuroimaging Initiative: Learning-based inference of longitudinal image changes: Applications in embryo development, wound healing, and aging brain. Proceedings of the National Academy of Sciences **122**(8), e2411492122 (2025)
10. LaMontagne, P.J., Benzinger, T.L., Morris, J.C., Keefe, S., Hornbeck, R., Xiong, C., et al.: OASIS-3: longitudinal neuroimaging, clinical, and cognitive dataset for normal aging and alzheimer disease. MedRxiv pp. 2019–12 (2019)
11. Li, H., Cieslak, M., Salo, T., Shinohara, R.T., Oathes, D.J., Davatzikos, C., Satterthwaite, T.D., Fan, Y.: Uncovering functional connectivity patterns predictive of cognition in youth using interpretable predictive modeling. Proceedings of the National Academy of Sciences **122**(42), e2505600122 (2025)
12. Li, H., Cui, Z., Cieslak, M., Salo, T., Moore, T.M., Gur, R.E., Gur, R.C., Shinohara, R.T., Oathes, D.J., Davatzikos, C., et al.: Spatial heterogeneity and subtypes of functional connectivity development in youth. Nature Communications (2026)
13. Li, H., Fan, Y.: Non-rigid image registration using fully convolutional networks with deep self-supervision (2017), https://arxiv.org/abs/1709.00799
14. Li, H., Fan, Y., Alzheimer's Disease Neuroimaging Initiative: Mdreg-net: Multi-resolution diffeomorphic image registration using fully convolutional networks with deep self-supervision. Human Brain Mapping **43**(7), 2218–2231 (2022)
15. Peng, H., Gong, W., Beckmann, C.F., Vedaldi, A., Smith, S.M.: Accurate brain age prediction with lightweight deep neural networks. Medical image analysis **68**, 101871 (2021)
16. Petersen, R.C., Aisen, P.S., Beckett, L.A., Donohue, M.C., Gamst, A.C., Harvey, D.J., Jack Jr, C.R., Jagust, W.J., Shaw, L.M., Toga, A.W., et al.: Alzheimer's disease neuroimaging initiative (ADNI) clinical characterization. Neurology **74**(3), 201–209 (2010)
17. Pombo, G., Gray, R., Cardoso, M.J., Ourselin, S., Rees, G., Ashburner, J., Nachev, P.: Equitable modelling of brain imaging by counterfactual augmentation with morphologically constrained 3D deep generative models. Medical Image Analysis **84**, 102723 (2023)
18. Raz, N., Rodrigue, K.M.: Differential aging of the brain: patterns, cognitive correlates and modifiers. Neuroscience & Biobehavioral Reviews **30**(6), 730–748 (2006)
19. Smith, S.M., Miller, K.L., Nichols, T.E.: Characterising ongoing brain aging and baseline effects from cross-sectional data. Imaging Neuroscience **3**, IMAG–a (2025)
20. Toepper, M.: Dissociating normal aging from Alzheimer's disease: A view from cognitive neuroscience. Journal of Alzheimer's disease **57**(2), 331–352 (2017)
21. Tustison, N.J., Avants, B.B., Cook, P.A., Zheng, Y., Egan, A., Yushkevich, P.A., Gee, J.C.: N4ITK: improved N3 bias correction. IEEE transactions on medical imaging **29**(6), 1310–1320 (2010)
22. Yin, C., Imms, P., Chowdhury, N.F., Chaudhari, N.N., Ping, H., Wang, H., Bogdan, P., Irimia, A., Alzheimer's Disease Neuroimaging Initiative: Deep learning to quantify the pace of brain aging in relation to neurocognitive changes. Proceedings of the National Academy of Sciences **122**(10), e2413442122 (2025)